Synthetic and Systems Biotechnology 9 (2024) 733–741

Contents lists available at ScienceDirect

Synthetic and Systems Biotechnology

journal homepage: www.keaipublishing.com/en/journals/synthetic-and-systems-biotechnology

Original Research Article

Identification of a human type XVII collagen fragment with high capacity for maintaining skin health

Xinglong Wang [a,b], Shuyao Yu [a,b], Ruoxi Sun [a,b], Kangjie Xu [a,b], Kun Wang [a,b], Ruiyan Wang [e], Junli Zhang [e], Wenwen Tao [e], Shangyang Yu [a,b], Kai Linghu [a,b], Xinyi Zhao [a,b], Jingwen Zhou [a,b,c,d,*]

[a] Engineering Research Center of Ministry of Education on Food Synthetic Biotechnology and School of Biotechnology, Jiangnan University, 1800 Lihu Road, Wuxi, Jiangsu, 214122, China
[b] Science Center for Future Foods, Jiangnan University, 1800 Lihu Road, Wuxi, Jiangsu, 214122, China
[c] Jiangsu Province Engineering Research Center of Food Synthetic Biotechnology, Jiangnan University, Wuxi, 214122, China
[d] School of Biotechnology, Jiangnan University, 1800 Lihu Road, Wuxi, 214122, China
[e] Bloomage Biotechnology Corporation Limited, 678 Tianchen Street, Jinan, Shandong, 250101, China

ARTICLE INFO

Keywords:
Type XVII collagen
Hair follicle stem cell differentiation
Higher-order assembly
Collagen recombinant expression

ABSTRACT

Collagen XVII (COL17) is a transmembrane protein that mediates skin homeostasis. Due to expression of full length collagen was hard to achieve in microorganisms, arising the needs for selection of collagen fragments with desired functions for microbial biosynthesis. Here, COL17 fragments (27–33 amino acids) were extracted and replicated 16 times for recombinant expression in *Escherichia coli*. Five variants were soluble expressed, with the highest yield of 223 mg/L. The fusion tag was removed for biochemical and biophysical characterization. Circular dichroism results suggested one variant (sample-1707) with a triple-helix structure at >37 °C. Sample-1707 can assemble into nanofiber (width, 5.6 nm) and form hydrogel at 3 mg/mL. Sample-1707 was shown to induce blood clotting and promote osteoblast differentiation. Furthermore, sample-1707 exhibited high capacity to induce mouse hair follicle stem cells differentiation and osteoblast migration, demonstrating a high capacity to induce skin cell regeneration and promote wound healing. A strong hydrogel was prepared from a chitosan and sample-1707 complex with a swelling rate of >30 % higher than simply using chitosan. Fed-batch fermentation of sample-1707 with a 5-L bioreactor obtained a yield of 600 mg/L. These results support the large-scale production of sample-1707 as a biomaterial for use in the skin care industry.

1. Introduction

Collagen is the most abundant protein in mammals, accounting for about 30 % of the total protein mass [1], and a fundamental component of the extracellular matrix of the skin, cartilage, tendon, brain, liver, lung, heart, kidney, and bone [2]. To date, 28 types of collagen have been identified and are classified based on molecular function, supramolecular organization, and distribution in tissues [3]. Collagen-based biomaterials are biocompatible and widely applied for repair of defects to cartilage, bone, and skin, in addition to dental implants [4]. Human collagen types I, II, III, V, X, and XVII are mainly used as components of skin care products, supplements, as well as various foods and beverages, with a global market value of 9.76 billion USD in 2023 (Report ID: GVR-1-68,038-835-0 from Grand View Research). Commercially available collagen is mainly extracted from animal tissues. However, due to the high price and low efficiency [5], more cost-effective sources of functional collagen for use as biomaterials are needed [6].

The use of genetic engineering technology with microorganisms to produce human collagen offers the advantages of low cost, clear genetic backgrounds, biocompatibility, biodegradability, and low risk of immune rejection [7,8]. Recombinant expression of human collagen in *Escherichia coli* was achieved by co-expressing proline hydroxylase to enable collagen self-assembly [9]. The resulting hydroxylated collagen formed a triple helix with a yield of 90 mg/L. Our group previously used a constitutive promoters to induce collagen recombinant expression,

Peer review under responsibility of KeAi Communications Co., Ltd.
* Corresponding author. Science Center for Future Foods, Jiangnan University, 1800 Lihu Road, Wuxi, Jiangsu, 214122, China.
E-mail address: zhoujw1982@jiangnan.edu.cn (J. Zhou).

https://doi.org/10.1016/j.synbio.2024.06.001
Received 5 March 2024; Received in revised form 4 June 2024; Accepted 5 June 2024
Available online 6 June 2024

obtaining a yield of 229 mg/L [10]. However, maintaining the triple-helix structure and bioactivity of naturally produced collagen remains challenging through microbial recombinant expression system. Therefore, it is important to identify collagen fragments resist to protease cleavage that are suitable for microbial expression and also able to self-assemble.

Type XVII collagen (COL17) is a type II transmembrane protein expressed in the epidermal basement membrane that influences differentiation of hair follicle stem cells (HFSCs) [11,12]. Expression of COL17 is strictly regulated, the downregulation of COL17 can lead to skin aging, atrophy, fragility, discoloration, and alopecia [13,14]. Similar to other types of collagen, COL17 assembles into a triple-helix structure relied on conserved G-X-Y repeats, where X and Y are mostly proline and hydroxyproline residues [12]. The bioactivity of COL17 is supported by functional domains, such as the collagenous domains, which are associated with hemidesmosomal and extracellular matrix proteins to maintain the skin health [15]. Biosynthesis of full length collagen with the use of microorganisms is challenging because the full-length molecule is insoluble [16]. The sequence composition and the structure of collagen are related to their bioactivities, highlighting the need to identify key functional domains of appropriate lengths for recombinant expression in microorganisms.

The aim of this study was to identify appropriate fragments of human COL17 with the ability for self-assembly and exhibiting COL17 functions, moreover, can be recombinant expression in *E. coli*. The COL17 fragments selected for recombinant expressed in *E. coli* varied in length from 27 to 33 amino acids. The fusion tag TrxA was used to benefit the soluble expression of COL17 variants and removed after purification. Circular dichroism (CD) was applied to confirm triple-helix assembly of the purified COL17 fragments. The capacity of the variants to form a higher-order structure was assessed by scanning electron microscopy (SEM), transmission electron microscopy (TEM), atom force microscopy (AFM), and viscoelasticity analysis. Also, *in vitro* and *in vivo* blood clotting tests and the bioactivity assay were conducted to evaluate the capacity of the identified COL17 variants to induce differentiation of osteoblasts and regeneration of skin cells. In addition, the swelling capacity of a hydrogel prepared using a complex of chitosan and a COL17 variant was evaluated.

2. Materials and methods

2.1. Study approval

The protocol of the animal study was approved by the Institutional Animal Care and Use Committee of Jiangnan University (JN. No. 20211030p0020301[431]), and conducted in accordance with the Guide for the Care and Use of Laboratory Animals (https://www.ncbi.nlm.nih.gov/books/NBK54050/).

2.2. Strains and plasmids

COL17 variants were expressed in *E. coli* BL21 (DE3) cells. The genes encoding for COL17 fragments were synthesized by GenScript Biotech Co., Ltd. (Nanjing, China) and ligated into a pET-32a(+) plasmid via *Kpn*I and *Blp*I restriction sites. The selected fragments (Table 1) were replicated 16 times for gene synthesis and recombinant expression (Table S1).

2.3. Recombinant expression

E. coli cells were transformed with pET-32a(+) carrying the expression cassettes of the COL17 variants. Single colonies obtained after transformation were cultivated in Luria–Bertani (LB) broth supplemented with ampicillin (50 μg/mL) at 37 °C for 10 h. The seed culture was cultivated in Terrific broth supplemented with ampicillin (50 μg/mL) at 37 °C. Protein induction by supplementation with 0.01 mM isopropyl β-D-1-thiogalactopyranoside (IPTG) and continued until the OD_{600} reached 1.2. Afterward, cultivation was continued at 20 °C for 20 h.

2.4. CD spectroscopy

For CD spectroscopy, the samples were diluted to 0.2 mg/mL in phosphate-buffered saline (PBS) at pH 7.5 and pre-incubated at 4 °C for 12 h. The CD spectra were obtained using Chirascan™ Circular Dichroism Spectrometer (Applied Photophysics Ltd., Leatherhead, UK) equipped with a Peltier temperature controller (model 110-OS; Hellma GmbH & Co. KG, Müllheim, Germany) with the use of quartz cuvettes (model 110-OS; optical path length, 1 mm; Hellma GmbH & Co. KG). The spectra were obtained at wavelengths 190–250 nm. The melting temperature (T_m) was calculated from standard curves obtained from changes in ellipticity at 220 nm during the heating process (0–70 °C at 1 °C/min).

2.5. Microscopy and analysis

For TEM analysis, samples were diluted to 1 mg/mL in PBS (pH 7.5) and incubated at 4 °C for 3 days. The sample solution was absorbed onto a copper grid for 1 min and excessive solvent was removed using filter paper. Samples were negatively stained with 0.75 % phosphotungstic acid prior to imaging using a transmission electron microscope (model H-7650; Hitachi High-Technologies Corporation, Tokyo, Japan). For SEM analysis, the samples were prepared at 3 mg/mL and incubated at 4 °C until hydrogel formation. Then, the samples were lyophilized and visualized with a scanning electron microscope (model SU8220; Hitachi High-Technologies Corporation). For AFM analysis, samples were prepared to 0.001 mg/mL and immobilized non-covalently on a hydrophilic mica surface to let air-dry of these samples. The AFM images were

Table 1
Properties of the COL17 variants analyzed in this study.

Sample no.	Sequence	Antimicrobial activity	Net charge at pH 7	Hydrophobicity	pI	T_m
1701	GPKGDRGPAGPPGHPGPPGPRGHKGEKGDK	2.48	3.18	0.25	11.21	−0.4
1702	GDRGPAGPPGHPGPPGPRGHKGEKGDKGDQ	2.77	1.18	0.31	10.12	7.1
1703	GDRGPAGPPGHPGPPGPRGHKGEKGDK	2.58	2.18	0.26	10.92	−2.7
1704	GEKGERGAAGEPGPHGPPGVPGSVGPKGSS	1.34	0.09	0.05	7.76	−17.8
1705	GLRGEVGLPGVKGDKGPMGPPGPKGDQGEK	1.47	1.00	0.08	10.12	0.2
1706	GEVGLPGVKGDKGPMGPPGPKGDQGEKGPR	1.63	1.00	0.11	10.12	11.7
1707	GLPGVKGDKGPMGPPGPKGDQGEKGPRGLT	1.46	2.00	0.07	10.92	10.1
1708	GVKGDKGPMGPPGPKGDQGEKGPRGLTGEP	1.85	1.00	0.16	10.12	13.4
1709	GDKGPMGPPGPKGDQGEKGPRGLTGEPGMR	2.22	1.00	0.16	10.12	12.8
1710	GPPGPPGPQGPKGDKGDPGVPGALGIP	0.37	−0.002	−0.17	6.75	22.8

The COL fragments were extracted using our developed python script.
The properties including antimicrobial activity, net charge, hydrophobicity, pI, and T_m were calculated using python peptides script.
The script for fragmentation and property evaluation was deposited in GitHub, at COL_extract folder:https://github.com/wangxinglong1990/COL_design.

obtained using a Dimension ICON (Bruker Optik GmbH, Leipzig, Germany). The sample width was measured using ImageJ software (https://imagej.net/ij/).

2.6. Cell cultivation

L929 fibroblasts (American Type Culture Collection, Manassas, VA, USA) were initially cultivated for 48 h in cultivating medium supplemented with 10 % (v/v) fetal bovine serum (Ausbian, Sydney, Australia) and 1 % (v/v) penicillin-streptomycin. Afterward, the cells were transferred to a new plate at 10^4 per well and cultivation was continued for 12 h to enable cell adhesion. Then, 10 mL of cultivating medium supplemented with 2 mg/mL of collagen sponges were added. Following cultivation for 48 h, the cells were counted using a CCK-8 Kit (Sangon Biotech Co. Ltd., Shanghai, China). The proliferation rate was calculated as the total number of cells after cultivation divided by the total number of cells before cultivation.

MC-3T3 cells and mouse hair follicle stem cells (HFSCs, American Type Culture Collection) were pre-cultivated in minimum essential medium (Gibco™; Invitrogen Trading (Shanghai) Co., Ltd., Shanghai, China) supplemented with 10 % (v/v) fetal bovine serum and 1 % (v/v) penicillin-streptomycin. Then, the cells (10^4/well) were loaded into the wells of a new plated and supplemented with 2 mg/mL of collagen sponges. The cells were cultivated for 12 h to allow for adhesion. Finally, the cells were washed with PBS and counted using a CCK-8 Kit. The adhesion rate was calculated as the number of adherent cells divided by the number of seeded cells.

2.7. Cell migration assay

For the cell migration assay [17], 5×10^5 MC-3T3 cells were plated and incubated to 95 % confluency. A scratch was made using pipette. Then, cultivating solution consisting of minimum essential medium supplemented with 10 % (v/v) fetal bovine serum and 1 % (v/v) penicillin-streptomycin with 2 mg/mL of collagen sponges was added. After 48 h, the scratch wound was imaged and calculated using ImageJ software.

2.8. Blood clotting test

The *in vitro* blood clotting test was conducted using platelet-poor plasma (Gibco, Shanghai, China) [18]. The blood was centrifuged at 2000×*g* for 10 min. Then, the supernatant was collected and supplemented with 2 mg/mL of collagen sponges. After incubation at 25 °C for 30 min, the supernatant was collected and quantified using a CCK-8 kit.

In vivo blood clotting assay using the mice (7–8 weeks), the tail of each mice was cut 1 cm from the tip. Collagen solution prepared at 2 mg/mL was applied to the wound. The process was recorded and the amount of bleeding was measured to evaluate the coagulation efficiency.

2.9. Real-time quantitative polymerase chain reaction (RT-qPCR)

Total RNA was extracted using TRIzol reagent (Invitrogen Corporation, Carlsbad, CA, USA), reverse-transcribed into complementary DNA using a One Step RT-qPCR Kit (Sangon Biotech Co. Ltd.), and quantified by RT-qPCR analysis using a QuantStudio3 RT-qPCR instrument (Thermo Fisher Scientific, Waltham, MA, USA) with the primers listed in Table S2. Gene expression levels were normalized against expression of glyceraldehyde-3-phosphate dehydrogenase (GAPDH).

2.10. Swelling rate calculation

Hydrogels were prepared by mixing chitosan with collagen sponges obtained in this study. Composite hydrogels (CC-25 % and CC-50 %) were prepared with 10 or 30 g of sample-1707 with 30 g of chitosan. Chitosan was dissolved in 1 % (v/v) acetic acid solution and then mixed with collagen sponges. The mixture was heated to 80 °C and then cooled down to room temperature for 1 h. The hydrogel was used to cultivate mouse blood at 25 °C and then washed with PBS. The swelling rate was calculated as the weight after incubation divided by the initial weight.

2.11. Fed-batch fermentation

Fed-batch fermentation was conducted using a 5-L bioreactor (T&J Bioengineering, Shanghai, China). *E. coli* cells were cultivated in 25 mL of LB medium for 12 h at 37 °C and then transferred to a 3-L fermentation system containing yeast extract, $(NH_4)_2SO_4$, KH_2PO_4, $K_2HPO4{\cdot}3H_2O$, $MgSO_4{\cdot}7H_2O$, monohydrate citric acid, vitamin B1, glycerol, and maltose dextrin (10, 5, 6,16.4, 1, 1.1, 0.1, 30, and 10 g/L, respectively) at pH 7.0. The supplements consisted of 3 g/L $MgSO_4{\cdot}7H_2O$, 10 g/L yeast extract, and 50 % (w/w) glycerol. During fermentation, pH was maintained at 7.0 by addition of NH_4OH (50 % v/v) and the dissolved oxygen content was maintained at 30 %. IPTG (1 mM) was added to the culture as needed.

3. Results

3.1. Selection, recombinant expression, and purification of COL17 fragments

In this study, we introduced a script to cleave fragments from collagen and predicted their biophysical properties (Table S3). Ten COL17 fragments consisting of 27–33 amino acids were selected. Among the selected fragments, the isoelectric point (pI) varied from 6.75 to 11.21 [19], T_m from −0.4 to 22.8 °C [20], hydrophobicity index from −0.17 to 0.31 [21], and bioactivity from 0.36 to 2.77 (Table 1) [22]. The selected fragments were replicated 16 times to recombinant express in *E. coli* and TrxA was fused to the N-terminal of the constructs for soluble expression (Fig. 1A). Five of the samples including 1705, 1706, 1707, 1708, and 1709 exhibited obvious bands in the soluble fraction. The yields of sample-1705 and sample-1708 were 195 and 223 mg/L, respectively. All samples were purified by affinity chromatography. Four of the samples including 1701, 1706, 1707, and 1708 exhibited obvious bands within the target area, and confirmed by matrix-assisted laser desorption/ionization time-of-flight mass spectrometry (MALDI--TOF MS) (Fig. 1B and Fig. S1).

The purified samples including 1701, 1704, 1706, and 1708 degraded more than 90 % at room temperature (~25 °C) after 12 h after purification as shown in Fig. 1C, while sample 1701 and 1704 completely degraded without detected band on SDS-PAGE. MALDI-TOF MS results confirmed the degradation of sample-1708 that degradation of TrxA and the cleaved fragments matched the fingerprint sequences (Fig. 1D). Therefore, only sample-1707 was further used as the research target. The fusion tag was removed by tobacco etch virus (TEV) protease cleavage and reverse purification using affinity chromatography. Notably, protease cleavage at 25 °C for 24 h, bands corresponding to sample-1707 and the TrxA tag were observed (Fig. 1E), demonstrating that the structure of sample-1707 was sufficiently stable to resist degradation.

3.2. Production of COL17 fragments in a 5-L bioreactor

Large-scale fed-batch fermentation in a 5-L bioreactor was conducted. Briefly, 250 mL of the starter culture were inoculated into a 2.5-L fermentation culture. The optical density at 600 nm (OD_{600}) value reached 40 by 12 h (Fig. 2A), followed by adding IPTG for induction and feeding supplements. Following induction, the OD_{600} value rapidly increased from 40 to 71 within the first 6 h and then slowly increased to 110 after 30 h (Fig. 2A). Samples were continuously collected after IPTG induction and visualized by sodium dodecyl-sulfate polyacrylamide gel electrophoresis (SDS-PAGE). A band corresponding to sample-1707

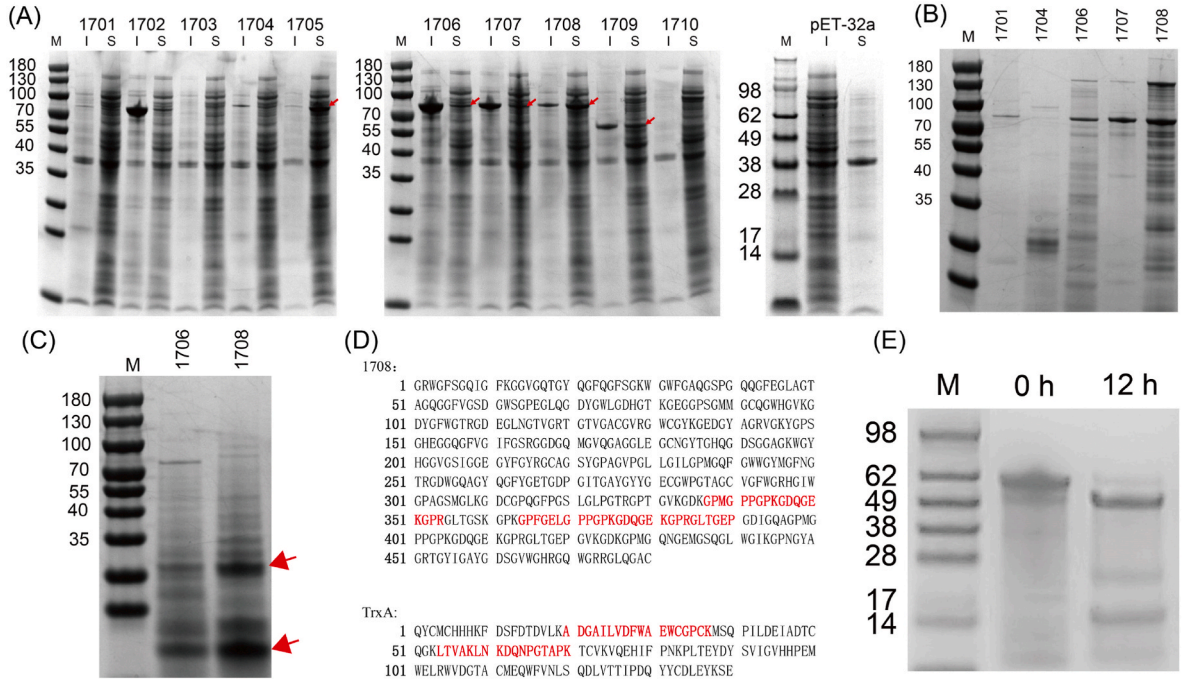

Fig. 1. Recombinant expression of COL17 fragments in *E. coli* cells.
(A) The soluble (S) and insoluble (I) fractions collected after cell lysis. The fractions for *E. coli* carried plasmid pET-32a was shown. (B) Purified samples from the soluble fraction. (C) Degradation process of samples 1706 and 1707 and visualized on SDS-PAGE. Notably, the thick band of sample 1701 and 1704 were fully degraded and not present on the gel. (D) MALDI-TOF MS analysis of the degraded band after incubation for 12 h, the upper and lower band indicated by red arrow in (C) were characterized that matched the sequence of 1708 and TrxA respectively. (E) Cleavage of the fusion tag of sample-1707 using the TEV protease.

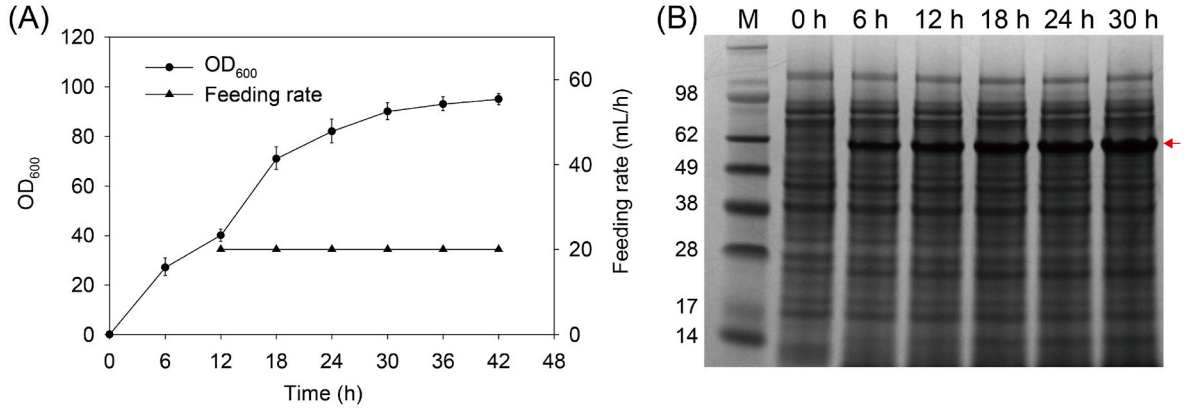

Fig. 2. Fed-batch fermentation using a 5-L bioreactor.
(A) OD_{600} values and feeding rates during fermentation. The starter culture (25 mL) was inoculated into the fermentation culture (3 L). Temperature was maintained at 20 °C after induction. The supplements consist of 3 g/L $MgSO_4{\cdot}7H_2O$, 10 g/L yeast extract, and 50 % (w/w) glycerol. (B) SDS-PAGE visualization of sample-1707 (indicated by red arrow). The time was counted after induction, sample 0 h and 6 h were diluted by 5-fold and 6-fold, while the following samples were diluted by 8-fold prior to loading in the gel.

emerged after 6 h of fermentation (Fig. 2B and Fig. S2). The yield of sample-1707 had stabilized from 12 to 30 h post-induction. The highest yield of sample-1707 was 600 mg/L.

3.3. Characterizing biophysical properties of sample-1707

Collagens form a triple-helix structure, which basically supports higher-order assemblies. CD analysis is a well-established technique to evaluate the triple-helix structure of collagens. The absence of a negative ellipticity band at 195 nm and the presence of a positive band at 220–222 nm suggested formation of a triple-helix structure [23]. The triple-helix structure of sample-1707 was confirmed by the appearance of the above two features, and we used murine COL1 as the positive control. The positive band of sample-1707 at 220–222 nm was visible at 25 °C and 37 °C, and a similar peak detected from COL1 as well (Fig. 3A). Gradually increasing the incubation temperature showed a triple-helix to untwisted structure transient at 43.2 °C for sample-1707 (Fig. 3B) [24].

To assess the capacity to assemble into a higher-order structure, sample-1707 was prepared to 1 mg/mL and incubated at 4 °C for 24 h. Subsequent TEM analysis confirmed the appearance of the obvious bands (Fig. 3C). The width of the formed nanofiber was measured indicated an average width of 5.6 nm (Fig. S3). Lyophilization of sample-1707 produced a porous collagen sponge that can be visualized at 5 μm scope (Fig. 3D). Moreover, sample-1707 was prepared to 0.001 mg/mL, and air-dried for AFM analysis, showing that less nanofibers

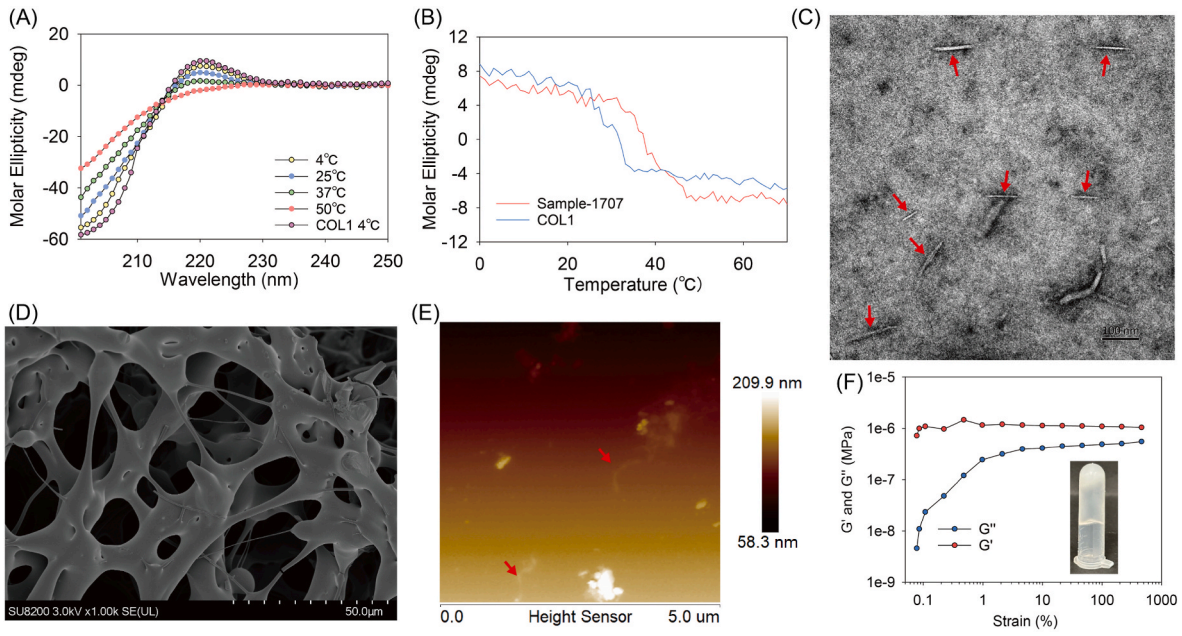

Fig. 3. Self-assembly of sample-1707.
(A) CD spectra of sample-1707 at different temperatures. (B) Melting curve of sample-1707 based on CD spectra. We used murine COL1 as a positive control during CD analysis as shown in (A) and (B). TEM (C), SEM (D), and AFM (E) images of sample-1707, the formed nanofibers were indicated by red arrow in (C) and (E). (F) The hydrogel prepared with sample 1707 at 3 mg/mL and viscoelasticity analysis using rheometry.

were detected at a relative low concentration, and the nanofibers formed aggregates (Fig. 3E). A collagen hydrogel was obtained by increasing the concentration of sample-1707 to 3 mg/mL (0.003 % w/v). Characterization of the formed hydrogel with a rheometer showed that the storage G' value was more than 2-fold greater than the loss G'' value, thereby demonstrating hydrogel formation (Fig. 3F) [25]. These results confirmed the transition of sample-1707 from an untwisted state to a triple-helix structure, followed by assembly into higher-order structures.

3.4. *In vivo and in vitro blood clotting tests*

Collagen-induced coagulation occurs by two pathways: collagen either binds to platelet receptors via endogenous hemostatic mechanisms or promotes the migration of fibroblasts to the wound site [26]. To validate the capacity of sample-1707 to facilitate blood clotting, *in vivo* and *in vitro* blood clotting tests were independently conducted. Commercial mouse COL1 was used as a reference. The samples were prepared as collagen sponges by lyophilization. An initial toxicity test showed that the proliferation rate of L929 fibroblasts with the use of bovine serum albumin (BSA), COL1, and sample-1707 were 177 %, 192 %, and 188 %, respectively (Fig. 4A). These results demonstrate that the samples were not toxic.

For the *in vitro* test, each sample was incubated with mouse blood that supplemented to 2 mg/mL. After incubation for 0.5 h at 25 °C and centrifugation [27], COL1 and sample-1707 induced clotting of blood cells by 80 % and 63 %, respectively (Fig. 4A). For the *in vivo* test, mouse tails were cleaved at 1 cm from the tip and treated with samples at a concentration of 2 mg/mL. The mice treated with commercial COL1

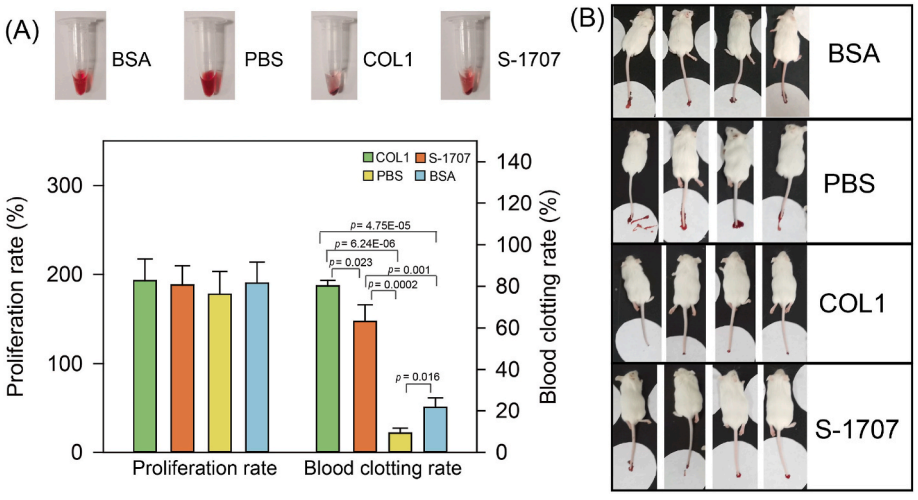

Fig. 4. Blood clotting test
(A) Cell proliferation rate of *in vitro* blood clotting rated based on commercial rat tail COL1, PBS (containing Ca^{2+}), BSA, and sample-1707 (S-1707). Cell proliferation based on L929 fibroblasts and cultivation for 48 h. Blood clotting after centrifugation in separate tubes. (B) *In vivo* blood clotting test based on mouse tail cleavage. The mouse tail was cleaved at 1 cm from the tip and treated with PBS (containing Ca^{2+}), COL1, BSA, or sample-1707. Blood loss was monitored for 10 min.

exhibited the smallest amount of blood loss, which was >1-fold less than the use of sample-1707, as determined with ImageJ software based on the bleeding area (Fig. 4B and Fig. S4). Meanwhile, the blood loss for mice treated by PBS and BSA was more than 3-fold higher than those treated with sample-1707. These results suggest that sample-1707 was capable for inducing coagulation, but displayed weaker activity than commercial COL1.

3.5. Bioactivity test

Collagen promotes bone regeneration by inducing differentiation of osteoblasts [7,28]. The capacity of sample-1707 to induce differentiation of MC-3T3 cells was assessed. The proliferation rates of MC-3T3 cells after 5 days of cultivation with commercial COL1, BSA, and sample-1707 were 327%–364 % (Fig. 5A). Cell adhesion assay was performed using MC-3T3 cells, and commercial COL1 and BSA were used as positive and negative control. After cultivation, the adhered cells were counted, indicating that both COL1 and sample-1707 promoted more than 1-fold higher cell adhesion rate than BSA, and the adhesion rate of COL1 was 30 % higher than that of sample-1707 (Fig. 5A—B). These results indicated that both commercial COL1 and sample-1707 can promote cell adhesion, but the activity of COL1 was higher.

The fibroblast differentiation were evaluated by measuring the mRNA levels of *VCL* and *ACTN* after on MC-3T3 cultivation [29,30]. Both COL1 and sample-1707 promoted transcription of *VCL* and *ACTN* (Fig. 5C), while the expression levels induced by COL1 were 101 % and 98 % greater than using of sample-1707. Meanwhile, the transcription level induced by sample-1707 was more than 70 % higher than that of BSA, confirming that sample-1707 can promote fibroblast differentiation. The cell migration test was conducted to further assess wound healing capacity based on MC-3T3 cells [17]. After 24 h cultivation, the wound gap decreased by > 60 % by treating with the three samples, respectively (Fig. S5). After 48 h, the original wound gap was covered by the migrated cells at 81 % and 83 % using BSA and COL1, and was full covered by sample-1707 (Fig. 5D).

The major contributions of COL17 are maintenance of hair follicle stem cells (HFSCs) and stabilization of epidermal patterns [14]. Overexpression of COL17 is related to the expression of nestin and SSEA1, which are critical for hair health [31]. So, the mRNA levels of *nestin* and *SSEA1* of mouse HFSCs cultured with COL1, BSA, and sample-1707 were measured. Expression of nestin and SSEA1 is considered a hallmark of the differentiation of HFSCs, and the process can take up to 28 days. Hence, HFSCs were cultivated with COL1, BSA, and sample-1707 and the mRNA levels of *nestin* and *SSEA1* were measured after 7 days. The mRNA expression levels of *nestin* and *SSEA1* were higher with the use of COL1 and sample-1707 than BSA (Fig. 5E). Moreover, the mRNA expression levels of *nestin* and *SSEA1* were 2.86- and 5.45-fold higher following cultivation with sample-1707 than COL1.

3.6. Swelling capacity of chitosan/sample-1707 complex

The hydrogel prepared with sample-1707 was not stable and did not convert into a solution phase by shaking or at temperatures greater than 20 °C. Therefore, a chitosan/collagen complex was used to strengthen the hydrogel and improve the swelling capacity [32]. Chitosan is approved for use in the food and cosmetic industries [33]. Hydrogels were prepared with sample-1707 at 25 % (10 g sample-1707 with 30 g chitosan) and 50 % (30 g sample-1707 with 30 g chitosan), respectively, obtaining CC-25 % and CC-50 %. Viscoelasticity analysis revealed that the differences among the storage G' values of CC-25 %, chitosan (3 % w/v), and sample-1707 (3 % w/v) were within 30 %, and the correlated loss G'' values were within 20 % (Fig. 6A). The storage G' value of CC-50 % was >80 % greater than the other three samples. In addition, storage G' values were > 5-fold greater than the loss G'' values for all samples (Fig. 6A). These results indicate that the CC-50 % hydrogel had the highest strength.

The structures of the hydrogels prepared with chitosan, CC-25 %, and CC-50 % were maintained at 25 °C. The swelling capacity of the

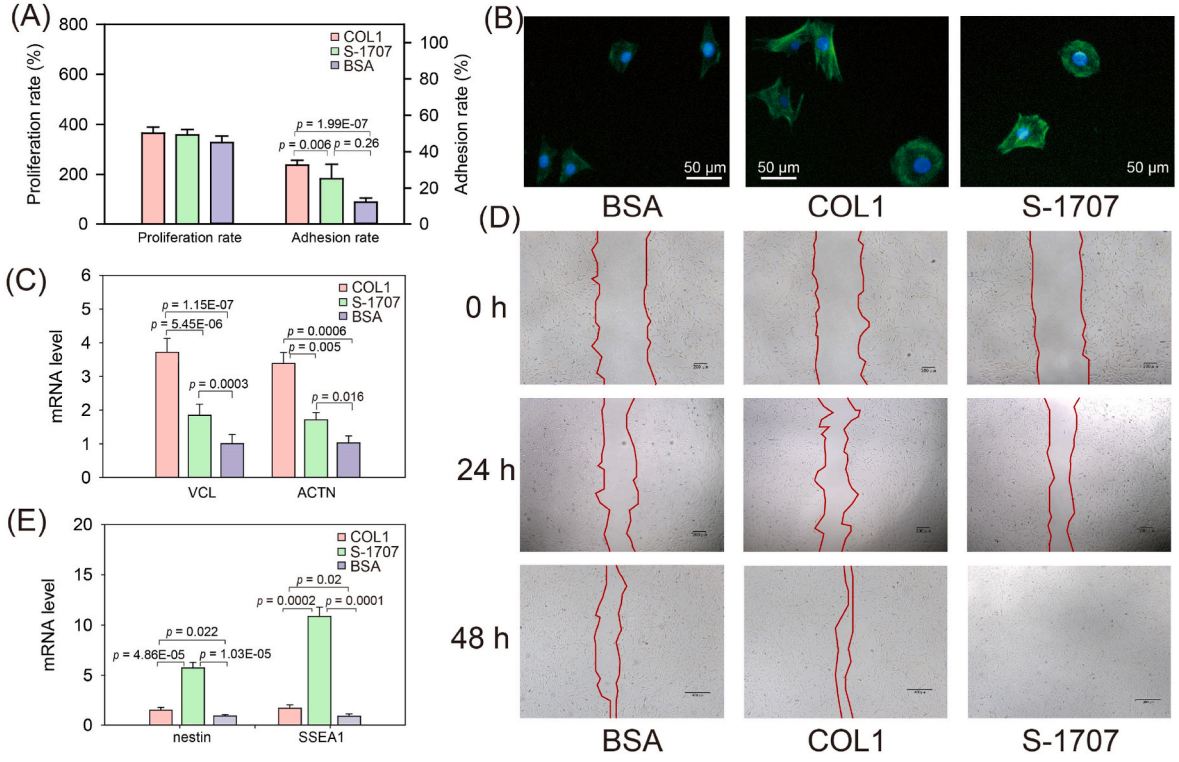

Fig. 5. Bioactivity of sample 1707.
(A) Cell proliferation and adhesion rates based on MC3T3-E1 cells. (B) Visualization of adhered MC3T3-E1 cells stained with phalloidin. (C) Detected mRNA levels of *VCL* and *ACTN* in MC3T3-E1 cells. (D) Cell migration test using MC3T3-E1 cells. (E) Detected mRNA levels of *nestin* and *SSEA1* in HFSCs. S-1707, sample-1707.

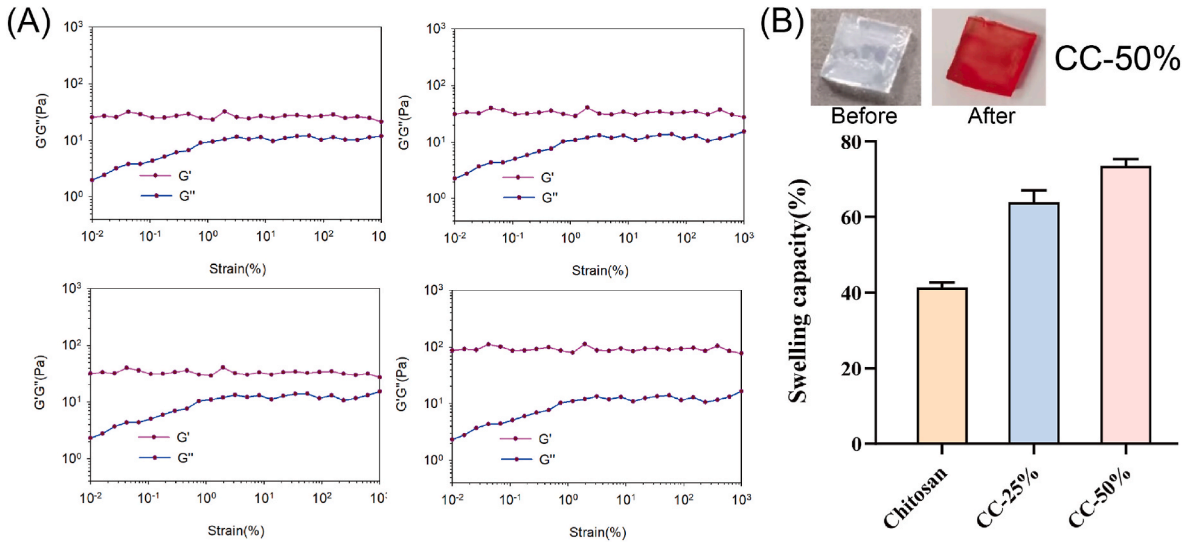

Fig. 6. Viscoelasticity analysis of mixtures of chitosan and sample-1707.
(A) Viscoelasticity analysis (rheometry) of chitosan and sample-1707. Chitosan and sample-1707 were independently prepared at 30 g/L. CC-25 % and CC-50 % were made by mixing 10 g and 30 g of sample-1707 with 30 g/L of chitosan. (B) The swelling rate was evaluated based on mouse blood. The hydrogel samples were prepared and incubated with mouse blood for 10 min "Before" and "After" indicate CC-50 % before and after incubation with mouse blood. After washing with PBS, the obtained total weight of the hydrogel was used to calculate the swelling rate.

hydrogels was evaluated by co-cultivating the hydrogel with mouse blood independently. After incubation at 25 °C for 10 min, the swelling capacity was evaluated by weighting the hydrogel that absorbed mouse blood. The results showed that the swelling capacities of the hydrogels prepared with CC-50 %, CC-25 %, and chitosan were 73 %, 65 %, and 41 %, respectively (Fig. 6B). These results demonstrate that chitosan combined with sample-1707 improved the swelling capacity of the obtained hydrogel.

4. Discussion

In this study, we developed a script for cleaving fragments from COL17 and attempted recombinant expression of 10 fragments independently in *E. coli*. Of these, five variants were soluble, while only one (sample-1707) maintained the triple-helix structure after purification and prolonged incubation at 25 °C. The triple-helix structure of sample-1707 was maintained at 37 °C (T_m = 43.2 °C) and exhibited higher-order assembly, as confirmed by SEM and TEM. Increasing the concentration of sample-1707 to 3 mg/mL facilitated conversion into a hydrogel. Moreover, sample-1707 induced differentiation of osteoblasts and skin cells. The use of chitosan with sample-1707 improved the swelling capacity of the hydrogen by >30 % as compared to chitosan alone. Fed-batch fermentation of sample-1707 using a 5-L bioreactor was optimal at a concentration of 600 mg/L. These results confirm that sample-1707 is a robust biomaterial and suitable for large-scale production using *E. coli*.

Human COL17 promotes regeneration of skin cells to help delay skin aging and hair loss [34]. Short fragments of COL could self-assemble into triple-helix [35,36], which supported its bioactivity as the whole COL molecule but can be easier produced using microorganisms [9,37]. Thus, we conducted fragments extraction and property prediction to assist the discovering of novel potential functional COL17 fragments, and successfully identified a functional COL17 variant. Comparing with previous COL sequential design strategies [7,24], this study focused on extracting fragments from native human COL. Even though the function of COL17 was long been reported [11,14], but the functional fragment search was firstly applied. Moreover, our result showed that the identified variant could benefit HFSCs differentiation mimicking the whole length of COL17 [31].

The bioactivity of the extracted collagen fragment ultimately determines potential usefulness for practical applications [38]. COL1 obtained from the rat tail was shown to promote blood clotting and is now commercially available as a hemostatic agent [39]. Although sample-1707 was found to promote coagulation and osteoblast differentiation, but with weaker performance than commerical COL1 [7]. Nonetheless, sample-1707 exhibited much stronger capacity to induce differentiation of HFSCs than COL1, which would be beneficial for repair and regeneration of hair follicles [40]. In addition, sample-1707 generated faster cell migration than COL1, which is critical for wound healing [17]. Overall, these results suggested that sample-1707 is a robust biocompatible material.

The capacity of sample-1707 to self-assemble from a triple helix to a higher-order structure was confirmed by CD, SEM, TEM, and viscoelasticity analysis. Notably, not all of the extracted fragments exhibited the capacity to self-assemble into a triple-helix structure, as reported here and in previous study [41]. The extracted fragments had a wide range of net charges, T_m, and hydrophobicity. However, the specific characteristic of sample-1707 responsible for the capacity to self-assemble remains elusive, thus warranting further studies. Lastly, large-scale fermentation of sample-1707 had unexpectedly terminated at 28 h post-induction, likely as a result of protease degradation and the fermentation method. Therefore, large-scale production must be optimized.

Data availability statement

The data supporting the findings of this study are available within the article and its Supplementary Information. Other data and reagents are available from the corresponding authors upon reasonable request.

CRediT authorship contribution statement

Xinglong Wang: conceived and designed the study and prepared the original draft. **Shuyao Yu:** performed the experiment. **Ruoxi Sun:** performed the experiment. **Kangjie Xu:** performed the experiment and analyzed the data. **Kun Wang:** performed the experiment. **Ruiyan Wang:** performed the experiment. **Junli Zhang:** provided technical help. **Wenwen Tao:** provided technical help. **Shangyang Yu:** performed the experiment. **Kai Linghu:** performed the experiment. **Xinyi Zhao:** performed the experiment. **Jingwen Zhou:** revised the original

draft, All authors have read and agreed to the published version of the manuscript.

Declaration of competing interest

The authors declare the following financial interests/personal relationships which may be considered as potential competing interests:

Co-author are the employees of Bloomage Biotechnology Corporation Limited - Ruiyan Wang, Junli Zhang, Wenwen Tao If there are other authors, they declare that they have no known competing financial interests or personal relationships that could have appeared to influence the work reported in this paper.

Acknowledgements

This study was funded by the Natural Science Foundation of Jiangsu Province (BK20202002), the Starry Night Science Fund of Zhejiang University Shanghai Institute for Advanced Study (Grant No. SN-ZJU-SIAS-0013), China Postdoctoral Science Foundation (2023M741403), Jiangsu Funding Program for Excellent Postdoctoral Talent (2023ZB037), the National First-class Discipline Program of Light Industry Technology and Engineering (QGJC20230102).

Appendix A. Supplementary data

Supplementary data to this article can be found online at https://doi.org/10.1016/j.synbio.2024.06.001.

References

[1] Tarnutzer K, Siva Sankar D, Dengjel J, Ewald CY. Collagen constitutes about 12% in females and 17% in males of the total protein in mice. Sci Rep 2023;13(1):4490. https://doi.org/10.1038/s41598-023-31566-z.

[2] Bielajew BJ, Hu JC, Athanasiou KA. Collagen: quantification, biomechanics and role of minor subtypes in cartilage. Nat Rev Mater 2020;5(10):730–47. https://doi.org/10.1038/s41578-020-0213-1.

[3] Gordon MK, Hahn RA. Collagens. Cell Tissue Res 2010;339(1):247–57. https://doi.org/10.1007/s00441-009-0844-4.

[4] Meyer M. Processing of collagen based biomaterials and the resulting materials properties. Biomed Eng Online 2019;18(1):24. https://doi.org/10.1186/s12938-019-0647-0.

[5] Chen Q, Pei Y, Tang K, Albu-Kaya MG. Structure, extraction, processing, and applications of collagen as an ideal component for biomaterials - a review. Collagen and Leather 2023;5(1):20. https://doi.org/10.1186/s42825-023-00127-5.

[6] Matinong AME, Chisti Y, Pickering KL, Haverkamp RG. Collagen extraction from animal skin. Biology 2022;11(6):905. https://doi.org/10.3390/biology11060905.

[7] Hu J, Li J, Jiang J, Wang L, Roth J, McGuinness KN, Baum J, Dai W, Sun Y, Nanda V, Xu F. Design of synthetic collagens that assemble into supramolecular banded fibers as a functional biomaterial testbed. Nat Commun 2022;13(1):6761. https://doi.org/10.1038/s41467-022-34127-6.

[8] Fertala A. Three decades of research on recombinant collagens: reinventing the wheel or developing new biomedical products? Bioengineering 2020;7(4). https://doi.org/10.3390/bioengineering7040155.

[9] Rutschmann C, Baumann S, Cabalzar J, Luther KB, Hennet T. Recombinant expression of hydroxylated human collagen in *Escherichia coli*. Appl Microbiol Biotechnol 2014;98(10):4445–55. https://doi.org/10.1007/s00253-013-5447-z.

[10] Xu K, Yu S, Wang K, Tan Y, Zhao X, Liu S, Zhou J, Wang X. AI and knowledge-based method for rational design of *Escherichia coli* Sigma70 promoters. ACS Synth Biol 2024;13(1):402–7. https://doi.org/10.1021/acssynbio.3c00578.

[11] Matsumura H, Mohri Y, Binh NT, Morinaga H, Fukuda M, Ito M, Kurata S, Hoeijmakers J, Nishimura EK. Hair follicle aging is driven by transepidermal elimination of stem cells via COL17A1 proteolysis. Science 2016;351(6273):aad4395. https://doi.org/10.1126/science.aad4395.

[12] Kirkness MWH, Lehmann K, Forde NR. Mechanics and structural stability of the collagen triple helix. Curr Opin Chem Biol 2019. https://doi.org/10.1016/j.cbpa.2019.08.001. 5398-105.

[13] McGrath JA, Gatalica B, Christiano AM, si K, Owaribe K, McMillan JR, Eady RAJ, Uitto J. Mutations in the 180–kD bullous pemphigoid antigen (BPAG2), a hemidesmosomal transmembrane collagen (COL17A1), in generalized atrophic benign epidermolysis bullosa. Nat Genet 1995;11(1):83–6. https://doi.org/10.1038/ng0995-83.

[14] Liu N, Matsumura H, Kato T, Ichinose S, Takada A, Namiki T, Asakawa K, Morinaga H, Mohri Y, De Arcangelis A, Geroges-Labouesse E, Nanba D, Nishimura EK. Stem cell competition orchestrates skin homeostasis and ageing. Nature 2019;568(7752):344–50. https://doi.org/10.1038/s41586-019-1085-7.

[15] Natsuga K, Watanabe M, Nishie W, Shimizu H. Life before and beyond blistering: the role of collagen XVII in epidermal physiology. Exp Dermatol 2019;28(10):1135–41. https://doi.org/10.1111/exd.13550.

[16] He J, Ma X, Zhang F, Li L, Deng J, Xue W, Zhu C, Fan D. New strategy for expression of recombinant hydroxylated human collagen α1(III) chains in *Pichia pastoris* GS115. Biotechnol Appl Biochem 2015;62(3):293–9. https://doi.org/10.1002/bab.1264.

[17] Xie W, Wu Q, Kuang Z, Cong J, Zhang Q, Huang Y, Su Z, Xiang Q. Temperature-Controlled expression of a recombinant human-like collagen I peptide in *Escherichia coli*. Bioengineering 2023;10(8). https://doi.org/10.3390/bioengineering10080926.

[18] Kumar VA, Taylor NL, Jalan AA, Hwang LK, Wang BK, Hartgerink JD. A nanostructured synthetic collagen mimic for hemostasis. Biomacromolecules 2014;15(4):1484–90. https://doi.org/10.1021/bm500091e.

[19] Rice P, Longden I, Bleasby A. EMBOSS: the European molecular biology open software suite. Trends Genet 2000;16(6):276–7. https://doi.org/10.1016/S0168-9525(00)02024-2.

[20] Walker DR, Hulgan SAH, Peterson CM, Li IC, Gonzalez KJ, Hartgerink JD. Predicting the stability of homotrimeric and heterotrimeric collagen helices. Nat Chem 2021;13(3):260–9. https://doi.org/10.1038/s41557-020-00626-6.

[21] Barley MH, Turner NJ, Goodacre R. Improved descriptors for the quantitative structure–activity relationship modeling of peptides and proteins. J Chem Inf Model 2018;58(2):234–43. https://doi.org/10.1021/acs.jcim.7b00488.

[22] Boman HG. Antibacterial peptides: basic facts and emerging concepts. J Intern Med 2003;254(3):197–215. https://doi.org/10.1046/j.1365-2796.2003.01228.x.

[23] Drzewiecki KE, Grisham DR, Parmar AS, Nanda V, Shreiber DI. Circular dichroism spectroscopy of collagen fibrillogenesis: a new use for an old technique. Biophys J 2016;111(11):2377–86. https://doi.org/10.1016/j.bpj.2016.10.023.

[24] Khare E, Yu C-H, Gonzalez Obeso C, Milazzo M, Kaplan DL, Buehler MJ. Discovering design principles of collagen molecular stability using a genetic algorithm, deep learning, and experimental validation. Proc Natl Acad Sci USA 2022;119(40):e2209524119. https://doi.org/10.1073/pnas.2209524119.

[25] Brazdaru L, Micutz M, Staicu T, Albu M, Sulea D, Leca M. Structural and rheological properties of collagen hydrogels containing tannic acid and chlorhexidine digluconate intended for topical applications. Compt Rendus Chem 2015;18(2):160–9. https://doi.org/10.1016/j.crci.2014.07.007.

[26] Mathew-Steiner SS, Roy S, Sen CK. Collagen in wound healing. Bioengineering 2021;8(5):63. https://doi.org/10.3390/bioengineering8050063.

[27] Luo Y, Tao F, Wang J, Chai Y, Ren C, Wang Y, Wu T, Chen Z. Development and evaluation of tilapia skin-derived gelatin, collagen, and acellular dermal matrix for potential use as hemostatic sponges. Int J Biol Macromol 2023:253127014. https://doi.org/10.1016/j.ijbiomac.2023.127014.

[28] Sbricoli L, Guazzo R, Annunziata M, Gobbato L, Bressan E, Nastri L. Selection of collagen membranes for bone regeneration: a literature review. Materials 2020;13(3):786. https://doi.org/10.3390/ma13030786.

[29] Peng X, Nelson ES, Maiers JL, DeMali KA. Chapter five - new insights into vinculin function and regulation. In: Jeon KW, editor. International review of cell and molecular biology. Academic Press; 2011. p. 191–231.

[30] Sjöblom B, Salmazo A, Djinović-Carugo K. α-Actinin structure and regulation. Cell Mol Life Sci 2008;65(17):2688. https://doi.org/10.1007/s00018-008-8080-8.

[31] Shirai K, Obara K, Tohgi N, Yamazaki A, Aki R, Hamada Y, Arakawa N, Singh SR, Hoffman RM, Amoh Y. Expression of anti-aging type-XVII collagen (COL17A1/BP180) in hair follicle-associated pluripotent (HAP) stem cells during differentiation. Tissue Cell 2019:5933–8. https://doi.org/10.1016/j.tice.2019.06.001.

[32] Azaza YB, van der lee A, Li S, Nasri M, Nasri R. Chitosan/collagen-based hydrogels for sustainable development: phycocyanin controlled release. Sustainable Chemistry and Pharmacy 2023:31100905. https://doi.org/10.1016/j.scp.2022.100905.

[33] Irastorza A, Zarandona I, Andonegi M, Guerrero P, de la Caba K. The versatility of collagen and chitosan: from food to biomedical applications. Food Hydrocolloids 2021:116106633. https://doi.org/10.1016/j.foodhyd.2021.106633.

[34] Nishie W, Natsuga K, Iwata H, Izumi K, Ujiie H, Toyonaga E, Hata H, Nakamura H, Shimizu H. Context-dependent regulation of collagen XVII ectodomain shedding in skin. Am J Pathol 2015;185(5):1361–71. https://doi.org/10.1016/j.ajpath.2015.01.012.

[35] Berisio R, Vitagliano L, Mazzarella L, Zagari A. Crystal structure of the collagen triple helix model [(Pro-Pro-Gly)10]3. Protein Sci 2002;11(2):262–70. https://doi.org/10.1110/ps.32602.

[36] San Antonio JD, Jacenko O, Fertala A, Orgel JPRO. Collagen structure-function mapping informs applications for regenerative medicine. Bioengineering 2021;8(1):3. https://doi.org/10.3390/bioengineering8010003.

[37] Ma L, Liang X, Yu S, Zhou J. Expression, characterization, and application potentiality evaluation of recombinant human-like collagen in Pichia pastoris. Bioresources and Bioprocessing 2022;9(1):119. https://doi.org/10.1186/s40643-022-00606-3.

[38] Joyce K, Fabra GT, Bozkurt Y, Pandit A. Bioactive potential of natural biomaterials: identification, retention and assessment of biological properties. Signal Transduct Targeted Ther 2021;6(1):122. https://doi.org/10.1038/s41392-021-00512-8.

[39] Yu P, Zhong W. Hemostatic materials in wound care. Burns & Trauma 2021: 9tkab019. https://doi.org/10.1093/burnst/tkab019.
[40] Chen P, Zhang F, Fan Z, Shen T, Liu B, Chen R, Qu Q, Wang J, Miao Y, Hu Z. Nanoscale microenvironment engineering for expanding human hair follicle stem cell and revealing their plasticity. J Nanobiotechnol 2021;19(1):94. https://doi.org/10.1186/s12951-021-00840-5.
[41] Tuusa J, Kokkonen N, Tasanen K. BP180/Collagen XVII: a molecular View. Int J Mol Sci 2021;2222. https://doi.org/10.3390/ijms222212233.